

Sketch-Guided Motion Diffusion for Stylized Cinemagraph Synthesis

Hao Jin¹, Hengyuan Chang¹, Xiaoxuan Xie¹, Zhengyang Wang¹, Xusheng Du¹,
Shaojun Hu², Haoran Xie¹

¹Japan Advanced Institute of Science and Technology (JAIST)

²Northwest A&F University

Figure 1. Given the input sketches with motion sketches (gradient greyscale lines) and text prompt, Sketch2Cinemagraph can automatically synthesize stylized cinemagraphs with the generated motion fields. The red font represents the text prompt for flow generation and the blue font for style generation. The gradient greyscale lines depict the flow motion direction. **(The generated stylized cinemagraphs are embedded and better viewed using Adobe Reader.)**

Abstract

Designing stylized cinemagraphs is challenging due to the difficulty in customizing complex and expressive flow motions. To achieve intuitive and detailed control of the generated cinemagraphs, freehand sketches can provide a better solution to convey personalized design requirements than only text inputs. In this paper, we propose Sketch2Cinemagraph, a sketch-guided framework that enables the conditional generation of stylized cinemagraphs from freehand sketches. Sketch2Cinemagraph adopts text prompts for initial content generation and provides hand-drawn sketch controls for both spatial and motion cues. The latent diffusion model is adopted to generate target stylized landscape images along with realistic versions. Then, a pre-trained object detection model is utilized to segment and obtain masks for the flow regions. We proposed a novel latent motion diffusion model to estimate the motion field in the fluid regions of the generated landscape images. The input motion sketches serve as the conditions to control the

generated vector fields in the masked fluid regions with the prompt. To synthesize the cinemagraph frames, the pixels within fluid regions are subsequently warped to the target locations for each timestep using a frame generator. The results verified that Sketch2Cinemagraph can generate high-fidelity and aesthetically appealing stylized cinemagraphs with continuous temporal flow from intuitive sketch inputs. We showcase the advantages of Sketch2Cinemagraph through quantitative comparisons against the state-of-the-art generation approaches.

1. Introduction

Cinemagraphs embody a captivating fusion of still photography and dynamical video, achieving a unique visual effect by seamlessly integrating motion into static images [4]. As a popular media format, cinemagraphs can exhibit a more lively and dynamic quality than static images. Additionally, Cinemagraphs can highlight movements against

a static background, providing more captivating and noticeable than videos. However, creating visually pleasing cinemagraphs demands considerable time and effort. It is challenging for amateurs to create cinemagraphs due to the required skills and experience in image editing and animation design. The traditional approaches for cinemagraph synthesis usually convert from video clips by detecting and extracting dynamic regions from frames while keeping other parts static [1, 53, 55, 56]. The other solutions include the estimation of physical properties of flow elements from static images to infer motion trajectories [15, 34, 42]. All these previous works require the source data with embedded motions or physically simulated actions.

Recently, the generative models including generate adversarial networks (GANs) [25] and diffusion models [39] have grasped widespread attention for their successes in creating captivating high-quality images and videos [3, 6, 20]. GAN inversion and deep feature warping were adopted for cinemagraph generation [6]. Text2Cinemagraph [32] can create artistic-styled cinemagraphs, which involves acquiring paired images in realistic and artistic domains using stable diffusion Model, followed by Eulerian displacement fields warping. Mahapatra and Kulkarni [31] animates the rasterized fluid elements by approximating the motion from user-provided flow hints. Li et al. [24] models the long-term motion prior in the Fourier domain and enables interaction with natural objects. These methods enhance the controllability of cinemagraphs, providing flexibility and precision in manipulating the visual contents. However, they have yet to explore more freeform approaches to creating cinemagraphs. Current options are limited to basic motion controls, like text and arrows, restricting the user’s ability to fully express their ideas. For content design, sketching is easily accessible and versatile for rapid prototyping of ideas and concepts [51]. Various sketch-based methods for image and video generation and editing have been developed [14, 27, 61]. To this end, this paper presents a novel framework that generates fluid elements and their motions from sketches to create personalized cinemagraphs.

In this work, we propose Sketch2Cinemagraph, a sketch-guided framework to generate stylized landscape cinemagraphs from the hand-drawn sketches as shown in Figure 1. Firstly, the proposed framework generates stylized landscape images with fluid elements and the corresponding realistic versions with the same spatial structure, conditioned on structural sketches and text that include both fluid and style prompts. Then, the motion field for fluid is estimated from the generated realistic landscape image, conditioning with motion sketches and fluid regions with text prompts using a diffusion model-based motion predictor. Finally, pixels in the stylized landscape image are warped to their future positions based on the motion field, resulting in visually pleasing cinemagraphs with specified styles.

In summary, our main contributions are listed as follows:

- A novel framework for landscape cinemagraph synthesis that uses a sketch-guided approach, to generate directly from freehand sketches with diffusion models.
- A fine-tuned latent diffusion model to generate realistic fluid elements, such as surging waterfalls, glittering sea, and ripple rivers from structural sketches.
- A diffusion-based motion prediction network to predict motion field from landscape image, conditioned on input motion sketches.

2. Related Work

2.1. Animation from still images

The challenge of animating still images is equivalent to simulating or reproducing the physically accurate visual features of natural objects in raster images. Several studies have focused on traditional physics-based natural objects simulation such as trees, rivers, clouds, smoke, and animal flocks, for animating scenery [7, 11, 15, 30, 52]. For predicting future frames, Walker et al. [48] propose a conditional variational autoencoder to precisely predict the dense trajectory of pixels in latent spaces. Logacheva et al. [29] propose a fine-tuned StyleGAN to mix realistic still images and timelapse videos prior for animating a given photograph. Fan et al. [9] simulate 2.5D transparent liquid via a combination of physics-based and learning-based methods. Recent studies have been incorporating Denoising Diffusion Probabilistic Models (DDPM) [12] into single-image animation tasks. AnimateDiff [10] proposes a practical pipeline that utilizes personalized text-guided image generative diffusion models for animation generation without specific fine-tuning. However, it struggles with maintaining consistency with real-world physical laws. Zhai et al. [57] integrates physics-aware simulation (PAS) with dual-flow texture learning (DFTL) to animate natural fluid effectively. Our method is dedicated to generating dynamic fluid elements with a continuous flowing structure.

2.2. Sketch-guided generative models

The sketch-guided generation tasks relevant to our work primarily focus on image and video generation. Chen and Hays [5] propose SketchyGAN, which is trained by augmented paired edge maps and photos to generate lifelike images from freehand sketches. Artistic images also can be generated from sketches conditioned on style images [26]. Recently, sketch-guided image generation using diffusion models has seen significant advancements. Voynov et al. [47] guide a pre-trained text-to-image diffusion model with a spatial map from the sketch domain during inference time. Peng et al. [35] propose a latent diffusion model trained by a two-stage process to achieve high-quality face synthesis. In the context of video generation, Zhang et al. [58] introduced

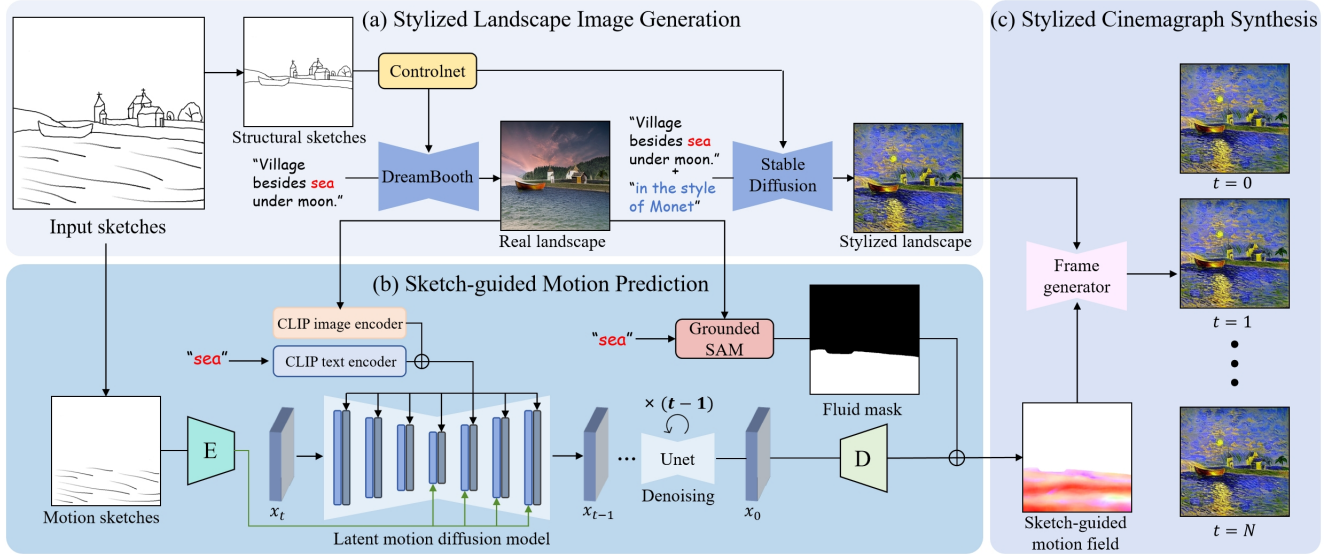


Figure 2. The Workflow of *Sketch2Cinemagraph*. Given input hand-drawn sketches of landscape structure and motions, the proposed framework can generate landscape cinemagraphs with (a) stylized landscape image generation, (b) sketch-guided motion field prediction, and (c) stylized cinemagraph synthesis steps.

a two-stage sketch-to-video generation method that allows users to create videos with two rough hand-drawn sketches. Li et al. [22] match a sketch with cartoon video frames and use a blending method to create a middle frame guided by the sketches. Instead of Interpolating frames, Zheng et al. [61] create abstract and dynamic sketches using Scalable Vector Graphics (SVG) within the input video. In contrast to static sketches, this study enables the creation of dynamic sketches.

2.3. Cinemagraph generation

Unlike videos, most frames in cinemagraphs remain static, with only certain elements animating in a seamless loop. Semi-automatic systems have been developed to loop the highlighted region of input videos [1, 16, 45, 53, 56]. Some require user guidance while others struggle with large underlined object movements. To address these issues, Oh et al. [33] proposed a semantic-aware-per-pixel optimization and human preference prediction to create cinemagraphs without user input. Endo et al. [8] created high-fidelity long-term waters and skies via convolutional neural networks (CNNs). Holynski et al. [13] predicted the optical flow maps of fluid regions and used deep warping pixels to generate continuous flow. To make motion predictor controllable, Mahapatra and Kulkarni [31] converted user-provided sparse arrow directions to dense flow via a flow-refinement network. StyleCineGAN [6] produced high-quality landscape cinemagraphs using warping multi-scale deep features within the latent space of pre-trained StyleGAN. In addition, artistic landscape cinemagraphs are gen-

erated by text-guided diffusion model and optical flow prediction [32]. To lift cinemagraphs into 3D space, Li et al. [23] presented 3D cinemagraphy which elevates 2D motion into 3D for animating landscape pictures. LoopGaussian [21] reconstructs 3D geometry from multi-view photos and inherent scene self-similarity with an Eulerian velocity field. Our work is similar to these landscape cinemagraph generation methods using a motion predictor to predict the motion fields of flow elements. However, our approach uniquely generates dynamic elements and a static background directly from simple sketches, thereby achieving full control over both the content and motion levels.

3. Method

In this work, we propose *Sketch2Cinemagraph*, a sketch-guided generation framework to synthesize the looping stylized landscape cinemagraphs from the hand-drawn sketches. Figure 2 illustrates the workflow of the proposed sketch-guided cinemagraph synthesis framework. For hand-drawn sketch inputs, we observe that **structural sketch** and **motion sketch** can be provided at different stages to separately design the landscape and cinemagraph motion. Motion sketch, the gradient greyscale lines depict the flow motion direction. For structural sketch, monoclar lines serves as spatical control.

The whole framework of *Sketch2Cinemagraph* consists of the following steps: stylized landscape image generation, sketch-guided motion prediction, and stylized cinemagraph synthesis. Firstly, at the stage of stylized landscape image generation as shown in Figure 2(a), a land-

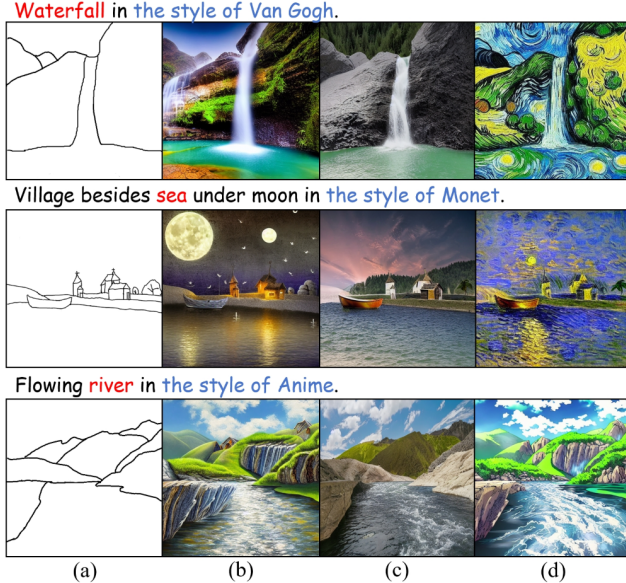


Figure 3. Paired Landscape image generation using fine-tuning stable diffusion model. The red text indicates landscape elements, and the blue text represents the provided style. (a) structural sketches; (b) landscape image generated by SD model; (c) photo-realistic landscape image generated by fine-tuned SD model; (d) landscape image in specific style generated by SD model.

scape image in the provided style and realistic one is generated from structural sketches conditioning with text prompt including the landscape elements, such as waterfall, sea, and river (Sec. 3.2). Subsequently, the masks for fluid elements are accurately extracted using the Segment Anything Model (SAM) [18] and applied to downstream motion field prediction tasks. For sketch-guided motion field as shown in Figure 2(b), a diffusion model-based motion field estimator accepts the realistic landscape image, text prompt, mask, and user-provided motion sketches to synthesize a motion field, which represents the flow trends of pixels in the fluid regions (Sec. 3.3). Finally, the looping frames of cinemagraphs are obtained via Euler integration and symmetric-splating in the stylized cinemagraph synthesis step as shown in Figure 2(c) (Sec. 3.4).

3.1. Preliminary: Text-to-Image Generation

The latent diffusion model (LDM) [39] generates high-quality images by applying the diffusion process in the embedding space rather than in the pixel space. Given an initial noise map $\epsilon \sim \mathcal{N}(0, I)$ sampled from a Gaussian distribution and conditioning vector c , for example text, sketch and depth map, an image I is generated through gradually removing noise through a denoising U-Net ϵ_θ in reverse diffusion steps. During training, latent diffusion models aim to minimize a denoising objective function by \mathcal{L} , which is

the loss function:

$$\mathcal{L} = \mathbb{E}_{x_0, c, \epsilon \sim \mathcal{N}(0, I), t} \left[\|\epsilon - \epsilon_\theta(x_t, t, c)\|_2^2 \right], \quad (1)$$

where t denotes a timestep uniformly sampled from $1, \dots, T$, and x_0 denotes the input image.

For spatial conditioning controls, ControlNet [59] augments large pre-trained text-to-image diffusion models with conditions including human pose, sketch, and depth. Instead of fine-tuning the entire model, the robust backbone is utilized to learn diverse conditional controls by freezing the deep encoding layers. Adding purpose-specific condition c_t to the conditioning set, the denoising network ϵ_θ learns to predict the noise added to the noisy image x_t . The loss function is designed to be as follows:

$$\mathcal{L} = \mathbb{E}_{x_0, c_t, c_f, \epsilon \sim \mathcal{N}(0, 1), t} \left[\|\epsilon - \epsilon_\theta(x_t, t, c_t, c_f)\|_2^2 \right], \quad (2)$$

where c_t denotes text prompts. The model can predict high-quality images by utilizing zero convolutions, which do not add noise to the network. In this paper, LDM is used to generate high-quality landscape images conditioned on specific style prompts.

3.2. Stylized Image Generation

The first step of *Sketch2Cinemagraph* aims to generate stylized landscape images and their realistic versions from the given structural sketch and text. We adopted the pre-trained stable diffusion model for image generation tasks. This state-of-the-art model can generate high-quality landscape paintings in the provided styles, as shown in Figure 3 (d). However, creating realistic landscape images remains challenging due to the insufficient quantity of high-quality landscape photographs in the training dataset. The baseline SD model has limitations in accurately generating naturalistic outdoor scenery from sketch inputs as shown in Figure 3 (b). In addition, retraining the stable diffusion models for our landscape generation task demands substantial computational resources.

To solve these issues, we fine-tune the stable diffusion model on a real landscape image dataset inspired by DreamBooth [40] for image personalization. In this work, we specifically focused on the scene images containing waterfalls, rivers, and seas. Then, the pre-trained ControlNet is employed to control the spatial regions and contents during the landscape image generation process. The output results successfully render photorealistic fluid elements, while maintaining coherent structure and composition, as shown in Figure. 3 (c).

For generating dynamic fluid elements while maintaining a still background, we extract the fluid mask from the generated landscape image. In order to automatically extract fluid masks with accurate edges from the generated landscape images, we utilize the Grounded Segment Anything Model [38] with text prompt, which integrates two

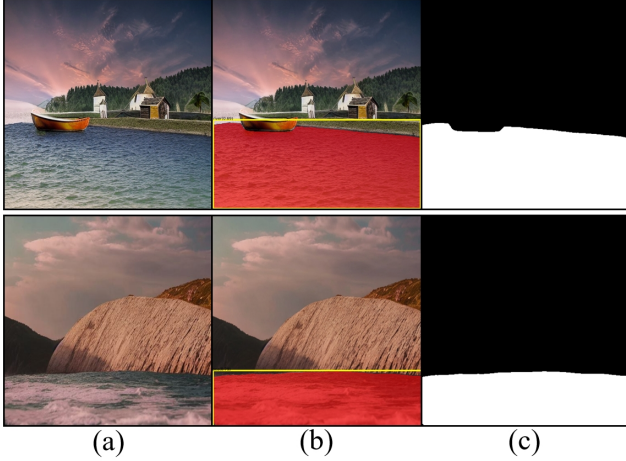


Figure 4. Two-stage fluid mask extraction results (c) from landscape images (a) using the bounding box (b) as intermediate detection results obtained from the Grounded SAM model.

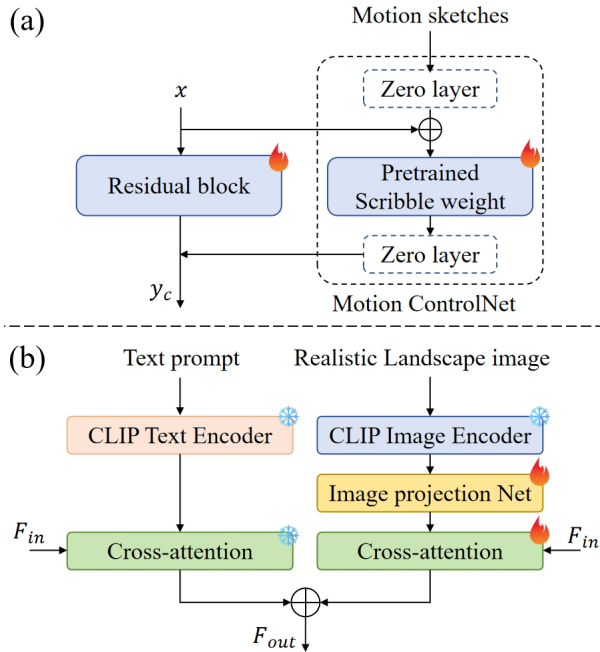


Figure 5. (a) ControlNet for motion sketches encoding; (b) New cross-attention layers for image features. The output F_{out} is fused from text and image embeddings.

large language models (LLMs): (1) Grounding DINO [28], an approach for detecting bounding boxes of arbitrary objects based on given text queries; (2) Segment Anything Model [17], which accepts the bounding boxes as input for generating a precise mask M . Figure 4 demonstrates the robust capability of the Grounded Segment Anything Model in accurately detecting text-guided fluid areas.

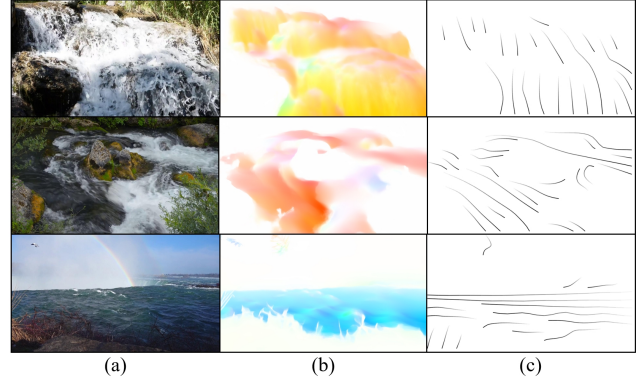


Figure 6. Examples in landscape dataset. (a) Landscape images; (b) Generated motion fields; (c) Extracted streamlines from motion fields which can serve as ground truth motion sketches.

3.3. Sketch-guided Motion Prediction

Motion Sketches. Different from the structural sketches used to control semantic structures in image generation. The motion sketches serve to control the movement of flow elements within the image. In this work, the motion sketches are created by resampling user-drawn lines to 20 points and smoothing. A gradient color from white to black is applied to the polyline vector to indicate motion direction.

Latent Motion Diffusion Model. To involve the motion dynamics in the fluid elements of the landscape image, we introduce latent motion diffusion model (LMDM) to predict a motion field from the generated realistic landscape image, conditioned on user-provided motion sketches and text prompt. The structure of the LMDM is shown in Figure 2(b). Initially, we train a CNN-based autoencoder for mapping the motion field into latent space, thereby applying the LDM to the motion field generation domain. To efficiently control the motion generation process using motion sketches, we train a ControlNet to encode sketches for guiding the flow direction of each pixel in the motion field. Simultaneously, to use the generated realistic landscape image and the text prompt as conditions, it is essential to project the referenced realistic landscape image into a shared embedding space that aligns semantically with the text embeddings. Inspired by IP-Adapter [54], we add a new cross-attention layer for each layer in the original U-Net model to incorporate image features. The semantic control is injected as follows, Z is the output of cross-attention:

$$Z = \text{Softmax}\left(\frac{\mathbf{Q}\mathbf{K}_t^T}{\sqrt{d}}\right)\mathbf{V}_t + \text{Softmax}\left(\frac{\mathbf{Q}\mathbf{K}_r^T}{\sqrt{d}}\right)\mathbf{V}_r \quad (3)$$

where K_t , V_t are the key and value matrices from the text features, K_r , V_r are the key and value matrices from the image features. The image cross-attention and text cross-attention use the same query \mathbf{Q} , as shown in Figure 5.

Dataset Preparation. We trained the motion field predictor on the same dataset in [13], which contains 4,750 paired videos and ground truth motion fields generated by Pwc-net [43]. For estimating motion fields from videos, we adopted VideoFlow [41], a state-of-the-art multi-frames optical flow generation framework, to regenerate the ground truth motion fields. Similar to [32], we used BLIP2 [19] to generate the captions of the first frame of each video, as the video content undergoes minimal changes. The ground truth motion sketches consist of streamlines extracted from the motion fields. The streamlines depict the movement direction of motion fields at any moment, which provides an intuitive visualization approach to represent the geometric structure and dynamics of motion fields. We first map the motion fields to grid-based velocity fields, with each grid containing x and y velocity components. The color and brightness information in motion fields are converted into the direction and magnitude of velocity. Runge-Kutta method was adopted to extract streamlines from generated velocity fields. We filtered the streamlines by velocity magnitude to simplify the motion sketches while preserving the main structure of the motion field. For motion sketches, a linear gradient ranging from white to black denotes the direction of the sketched motions. Figure 6 presents examples from the dataset, including the original landscape image, manually annotated motion sketches overlaid on the fluid region, and the corresponding motion field of the original image.

After the network predicts the motion field F_M from the generated landscape image, it can be used to compute the new two-dimensional position of each original pixel P_0 in the n -th frame to the next frame, where $n \in \{0, 1, \dots, N\}$.

$$P_{n+1} = P_n + F_M(P_n), F_M(P_n) = F_{n \rightarrow n+1}(P_n), \quad (4)$$

Similar to [13], We adopt the Euler integration method to reduce the number of model inference iterations,

$$F_{0 \rightarrow n}(\hat{P}_0) = F_{0 \rightarrow n-1}(\hat{P}_0) + F_M(\hat{P}_0 + F_{0 \rightarrow n-1}(\hat{P}_0)), \quad (5)$$

where displacement field $F_{0 \rightarrow n}$ enables direct pixels relocation, allowing pixels from the initial frame to be moved at their corresponding location \hat{P}_0 in the target n -th frame. However, directly warping in the pixel space results in large unknown holes overtime at the edge of fluid regions.

3.4. Cinemagraph Generation

The seamless looping cinemagraph can be synthesized with symmetric splatting in the deep space [13]. Specifically, the displacement fields are applied to bidirectional warp the deep feature map D_0 to D_{-n} and D_n , utilizing a softmax function to determine the contributions of colliding source pixels in the target frame:

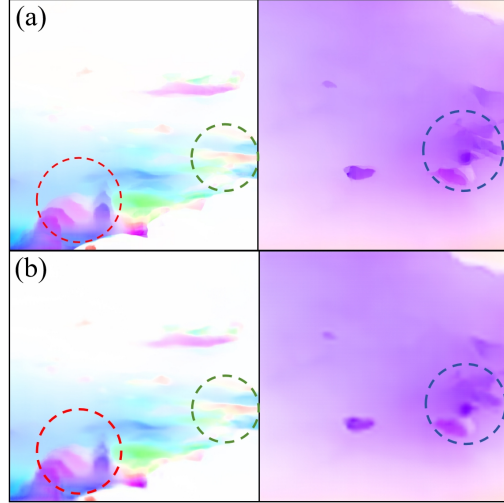


Figure 7. Examples of motion fields reconstructed by our motion autoencoder. The reconstructed results (b) effectively retain the motion information from the ground truth motion fields (a).

$$D_n(\hat{p}) = \frac{\sum_{p \in \mathcal{P}} \alpha D_n(p) e^{Z(p)} + \sum_{\hat{p} \in \hat{\mathcal{P}}} \hat{\alpha} D_{n-N}(\hat{p}) e^{Z(\hat{p})}}{\sum_{p \in \mathcal{P}} \alpha e^{Z(p)} + \sum_{\hat{p} \in \hat{\mathcal{P}}} \hat{\alpha} e^{Z(\hat{p})}} \quad (6)$$

where $\alpha = 1 - \frac{n}{N}$ and $\hat{\alpha} = \frac{n}{N}$, \mathcal{P} and $\hat{\mathcal{P}}$ denote two sets of pixels which bidirectional map to the same destination pixel. Then, the feature map set $D = \{D_{-N}, D_{-(N-1)}, \dots, D_0, \dots, D_{N-1}, D_N\}$ are decoded and transformed into the pixel space, resulting in the frame set $I = \{I_{-N}, I_{-(N-1)}, \dots, I_0, \dots, I_{N-1}, I_N\}$. The final output cinemagraph is composed by combining these individual frames. We adopt a U-Net-based frame generator [32] to conduct symmetric splatting in the feature space of the encoder component of the generator. Subsequently, the decoder component is utilized to generate the RGB image from the encoded features. The frame generator is trained on the existing landscape dataset [13]. In this work, we directly employed the pre-trained network for cinemagraph synthesis. Experiments demonstrate that this network can generate seamless cinemagraphs.

4. Implementation Details

We conducted all experiments with Intel i9-12900k 4.8GHz and GeForce RTX A6000 GPU. The neural networks were implemented using Diffusers [46] with PyTorch 1.13. LMDM was implemented based on Stable Diffusion(SD) v1.5 [39]. To adapt the diffusion model for motion field generation, we replaced AutoencoderKL with a lightweight motion Autoencoder which consists of an encoder and a

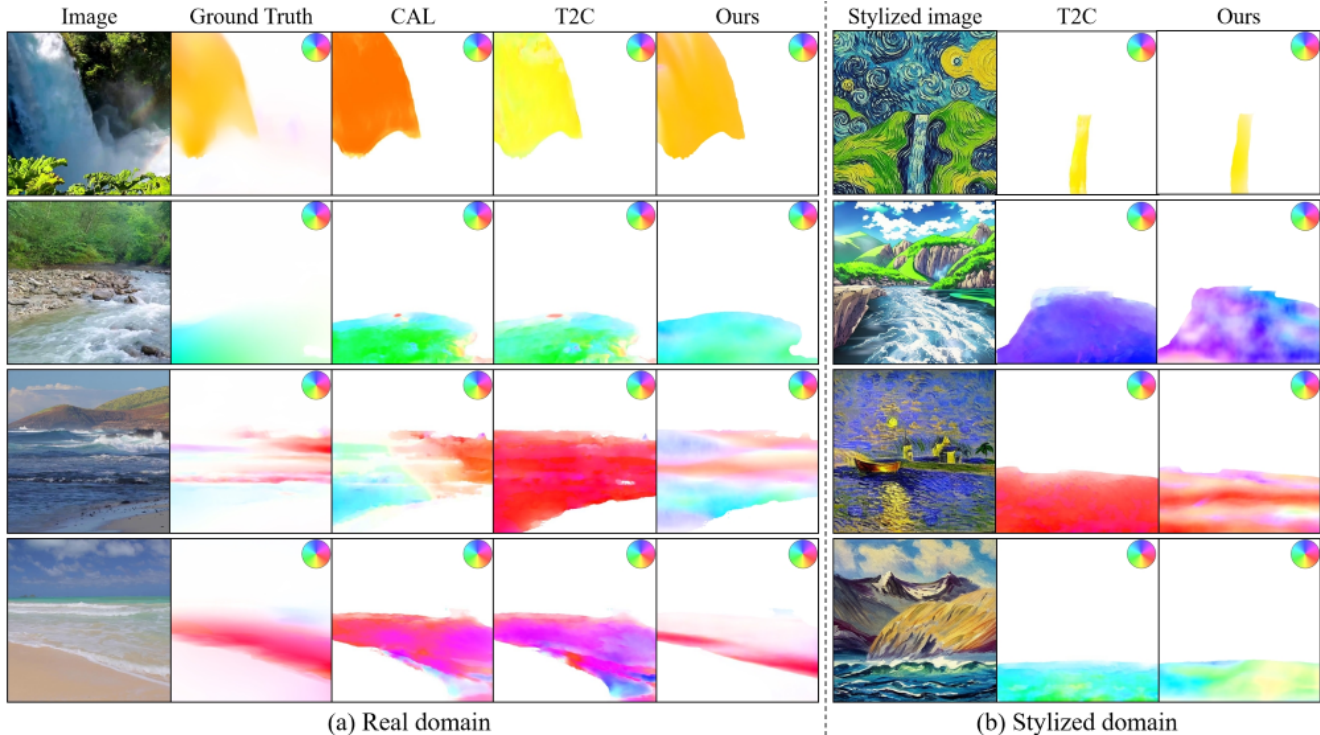


Figure 8. Visual comparisons with CAL for motion field prediction demonstrate that our LMDM generates more realistic motions that better align with target ground truth. Additional video comparisons with more baselines are available in our supplement.

decoder. The encoder, comprising six convolutional layers with ReLU activation, compressed the motion field in $2 \times 512 \times 512$ into a compact $4 \times 64 \times 64$ size. The decoder can reconstruct it back to the original motion field, preserving the essential motion details as shown in Figure 7. The motion Autoencoder was trained on the motion fields generated by VideoFlow using the landscape dataset with endpoint-error (AEPE) and mean squared error (MSE) loss.

The training of LMDM consists of two stages. In the first stage, a ControlNet was trained to extract the feature of motion sketches which were used as conditions to injected into the denoising step of LMDM. To reduce the number of training epochs, We inverted the colors of the ground truth of motion sketches and continued training using the provided scribble condition weights [59], as well as the denoising U-Net in SD v1.5. After training the ControlNet, a novel cross-attention layer for image features was added to the denoising U-Net. In the second stage, the first frame of each video was encoded by the image encoder of CLIP [37], and then projected to the text embeddings space by an image project model using Multi-Layer Perceptron (MLP) network. During training, the weights of ControlNet and U-Net from the previous stage were frozen, while the weights of the cross-attention layers for image features and the image projection model were updated. The paired data in the dataset were randomly cropped to 512×512 resolution. We

employed the AdamW optimizer with a constant learning rate of 5×10^{-6} for training all models.

5. Experiments

5.1. Qualitative Evaluation

We qualitatively evaluated our sketch-guided LMDM’s ability for flexible control of the movement of stylized cinemagraphs. Figure 9 shows the motion field generated using different input motion sketches. We observed that the flow motion closely matches the input motion sketches, demonstrating the robustness and flexibility of our proposed model in generating motion fields from motion sketches.

Similar to CAL [31], recent methods for controllable cinemagraph generation [6, 23] convert sparse hints into dense motion fields. Therefore, we compare our sketch-guided LMDM with CAL regarding motion quality. Since these two methods use different motion control conditions, we extract five hints and streamlines from the ground truth motion field to ensure an objective comparison under identical motion conditions. The extracted hints and streamlines are used as motion control conditions for both the CAL method and our LMDM method during evaluation. This consistency helps reduce result bias caused by differences in control conditions. In addition, we compare our method with Text2Cinemagraph (T2C), which enables the

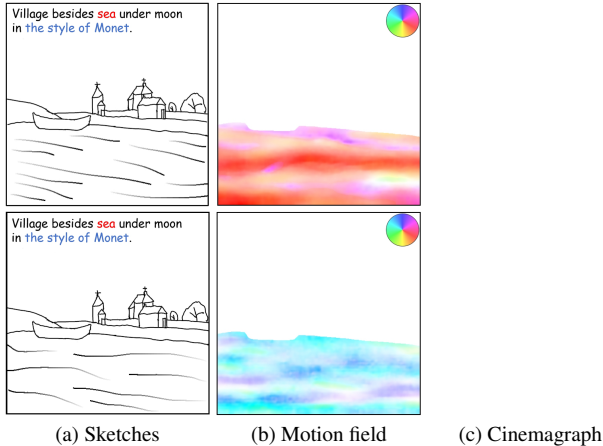


Figure 9. Example of motion field generation with different motion sketches for the same stylized landscape image. This demonstrates the robustness and flexibility of our LMDM to arbitrary input directions guided by motion sketches.

generation of cinemagraphs with text-guided motion direction control. Simultaneously, we used the fluid mask extracted from the real motion field as the constraint region for the three models. The comparison of the generated motion fields is shown in Figure 8. The motion fields generated by our LMDM closely matched the ground truth. In contrast, the T2C and CAL methods struggle to accurately generate motion fields for fluids with complex flow patterns, such as oceans with waves or rivers with ripples. However, for simpler flow patterns like waterfalls or calm seas, all three methods can successfully maintain the correct flow direction. This demonstrates that our method excels in handling fluids with intricate and variable flow characteristics. Therefore, sketch-guided LMDM provides greater flexibility and more precisely captures user intentions compared to hint and text guidance. By given the motion sketches. Figure 10 shows "campfire and smoke" cinemagraphs in various styles generated from the same structural and motion sketches. This demonstrates that our model performs well not only in stylized domains but also in realistic domains.

5.2. Quantitative Evaluation

To evaluate the quality of generated motion field, we choose Peak Signal-to-Noise Ratio (PSNR), Multi-Scale Structural Similarity (MS-SSIM) [49], AEPE, and MSE to measure the similarity between the generated motion field and the ground truth. Table 1 demonstrates that our sketch-based LMDM generates motion fields more closely align with the target ground truth than CAL and T2C method.

We evaluate the generated cinemagraphs against ground-truth videos using Frechet Video Distance (FVD) with the pre-trained I3D [44] model and LPIPS [60] with the AlexNet model. Table 2 shows that our method achieves

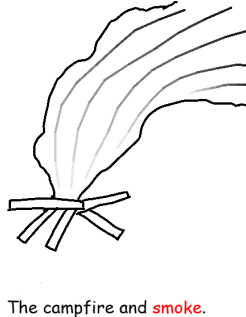


Figure 10. Various stylized cinemagraphs were generated using the same structural and motion sketches.

Table 1. Quantitive comparisons regarding motion field quality. Here we compare the generated motion fields with ground truth regarding PSNR, MS-SSIM, AEPE and MSE.

Method	PSNR \uparrow	MS-SSIM \uparrow	AEPE \downarrow	MSE \downarrow
CAL	16.8566	0.8053	0.2589	0.1607
T2C	15.2333	0.7481	0.3227	0.2103
Ours	21.4019	0.8440	0.2532	0.1557

Table 2. Quantitive comparisons cinemagraphs with ground truth videos regarding FVD and LPIPS.

Method	FVD \downarrow	LPIPS \downarrow
CAL	1616.76	0.1659
T2C	1884.82	0.2418
Ours	1535.99	0.1567

lower FVD and LPIPS scores than CAL and T2C, highlighting a closer match in fluid movement and visual fidelity compared to the ground-truth videos.

6. Conclusions

This paper proposed Sketch2Cinemagraph, a sketch-guided generation framework for stylized landscape cinemagraphs from freehand sketches. This method can generate visually appealing cinemagraphs based on user-provided structural and motion sketches with intuitive control. This approach enables amateur users without design skills to create landscape cinemagraphs and makes cinemagraph creation ac-

cessible to a broader audience. Through evaluation experiments, we demonstrated that our method outperforms all baseline approaches. For limitations, our approach is unsuitable for simulating realistic fluids as other cinemagraph synthesis work [13, 32]. When generating landscape images, the pre-trained stable diffusion model may generate the unwanted objects like rocks or ships in the fluid regions. To address this issue, alternative seed values are required to generate images that accurately match the flow structure.

References

- [1] Jiamin Bai, Aseem Agarwala, Maneesh Agrawala, and Ravi Ramamoorthi. Automatic cinemagraph portraits. In *Computer Graphics Forum*, pages 17–25. Wiley Online Library, 2013. 2, 3
- [2] Simon Baker, Daniel Scharstein, James P Lewis, Stefan Roth, Michael J Black, and Richard Szeliski. A database and evaluation methodology for optical flow. *International journal of computer vision*, 92:1–31, 2011. 1
- [3] Hugo Bertiche, Niloy J Mitra, Kuldeep Kulkarni, Chun-Hao P Huang, Tuanfeng Y Wang, Meysam Madadi, Sergio Escalera, and Duygu Ceylan. Blowing in the wind: Cyclenet for human cinemagraphs from still images. In *Proceedings of the IEEE/CVF Conference on Computer Vision and Pattern Recognition*, pages 459–468, 2023. 2
- [4] Kevin Burg and Jamie Beck. Introduction to bayesian statistics, 2011. 1
- [5] Wengling Chen and James Hays. Sketchygan: Towards diverse and realistic sketch to image synthesis. In *Proceedings of the IEEE conference on computer vision and pattern recognition*, pages 9416–9425, 2018. 2
- [6] Jongwoo Choi, Kwanggyoon Seo, Amirsaman Ashtari, and Junyong Noh. Stylecinegan: Landscape cinemagraph generation using a pre-trained stylegan, 2024. 2, 3, 7
- [7] Yung-Yu Chuang, Dan B Goldman, Ke Colin Zheng, Brian Curless, David H Salesin, and Richard Szeliski. Animating pictures with stochastic motion textures. In *ACM SIGGRAPH 2005 Papers*, pages 853–860. 2005. 2
- [8] Yuki Endo, Yoshihiro Kanamori, and Shigeru Kuriyama. Animating landscape: self-supervised learning of decoupled motion and appearance for single-image video synthesis. *ACM Transactions on Graphics (Proc. of SIGGRAPH ASIA 2019)*, 38(6):175:1–175:19, 2019. 3
- [9] Siming Fan, Jingtian Piao, Chen Qian, Hongsheng Li, and Kwan-Yee Lin. Simulating fluids in real-world still images. In *Proceedings of the IEEE/CVF International Conference on Computer Vision*, pages 15922–15931, 2023. 2
- [10] Yuwei Guo, Ceyuan Yang, Anyi Rao, Zhengyang Liang, Yaohui Wang, Yu Qiao, Maneesh Agrawala, Dahua Lin, and Bo Dai. Animatediff: Animate your personalized text-to-image diffusion models without specific tuning. *International Conference on Learning Representations*, 2024. 2
- [11] Ralf Habel, Alexander Kusternig, and Michael Wimmer. Physically guided animation of trees. In *Computer Graphics Forum*, pages 523–532. Wiley Online Library, 2009. 2
- [12] Jonathan Ho, Ajay Jain, and Pieter Abbeel. Denoising diffusion probabilistic models. *Advances in neural information processing systems*, 33:6840–6851, 2020. 2
- [13] Aleksander Holynski, Brian L Curless, Steven M Seitz, and Richard Szeliski. Animating pictures with eulerian motion fields. In *Proceedings of the IEEE/CVF Conference on Computer Vision and Pattern Recognition*, pages 5810–5819, 2021. 3, 6, 9
- [14] Zhengyu Huang, Haoran Xie, Tsukasa Fukusato, and Kazunori Miyata. Anifacedrawing: Anime portrait exploration during your sketching. In *ACM SIGGRAPH 2023 Conference Proceedings*, 2023. 2
- [15] Wei-Cih Jhou and Wen-Huang Cheng. Animating still landscape photographs through cloud motion creation. *IEEE Transactions on Multimedia*, 18(1):4–13, 2015. 2
- [16] Neel Joshi, Sisil Mehta, Steven Drucker, Eric Stollnitz, Hugues Hoppe, Matt Uyttendaele, and Michael Cohen. Clippets: juxtaposing still and dynamic imagery. In *Proceedings of the 25th annual ACM symposium on User interface software and technology*, pages 251–260, 2012. 3
- [17] Alexander Kirillov, Eric Mintun, Nikhila Ravi, Hanzi Mao, Chloe Rolland, Laura Gustafson, Tete Xiao, Spencer Whitehead, Alexander C. Berg, Wan-Yen Lo, Piotr Dollár, and Ross Girshick. Segment anything. *arXiv:2304.02643*, 2023. 5
- [18] Alexander Kirillov, Eric Mintun, Nikhila Ravi, Hanzi Mao, Chloe Rolland, Laura Gustafson, Tete Xiao, Spencer Whitehead, Alexander C Berg, Wan-Yen Lo, et al. Segment anything. In *Proceedings of the IEEE/CVF International Conference on Computer Vision*, pages 4015–4026, 2023. 4
- [19] Junnan Li, Dongxu Li, Silvio Savarese, and Steven Hoi. Blip-2: Bootstrapping language-image pre-training with frozen image encoders and large language models. In *International conference on machine learning*, pages 19730–19742. PMLR, 2023. 6
- [20] Jiyang Li, Lechao Cheng, Zhangye Wang, Tingting Mu, and Jingxuan He. Loopgaussian: Creating 3d cinemagraph with multi-view images via eulerian motion field. *arXiv preprint arXiv:2404.08966*, 2024. 2
- [21] Jiyang Li, Lechao Cheng, Zhangye Wang, Tingting Mu, and Jingxuan He. Loopgaussian: Creating 3d cinemagraph with multi-view images via eulerian motion field. *arXiv preprint arXiv:2404.08966*, 2024. 3
- [22] Xiaoyu Li, Bo Zhang, Jing Liao, and Pedro V Sander. Deep sketch-guided cartoon video inbetweening. *IEEE Transactions on Visualization and Computer Graphics*, 28(8):2938–2952, 2021. 3
- [23] Xingyi Li, Zhiguo Cao, Huiqiang Sun, Jianming Zhang, Ke Xian, and Guosheng Lin. 3d cinemagraphy from a single image. In *Proceedings of the IEEE/CVF Conference on Computer Vision and Pattern Recognition*, pages 4595–4605, 2023. 3, 7
- [24] Zhengqi Li, Richard Tucker, Noah Snively, and Aleksander Holynski. Generative image dynamics. In *Proceedings of the IEEE/CVF Conference on Computer Vision and Pattern Recognition (CVPR)*, 2024. 2
- [25] Wentong Liao, Kai Hu, Michael Ying Yang, and Bodo Rosenhahn. Text to image generation with semantic-spatial

- aware gan. In *Proceedings of the IEEE/CVF conference on computer vision and pattern recognition*, pages 18187–18196, 2022. 2
- [26] Bingchen Liu, Kunpeng Song, Yizhe Zhu, and Ahmed Elgammal. Sketch-to-art: Synthesizing stylized art images from sketches. In *Proceedings of the Asian Conference on Computer Vision*, 2020. 2
- [27] Feng-Lin Liu, Shu-Yu Chen, Yu-Kun Lai, Chunpeng Li, Yue-Ren Jiang, Hongbo Fu, and Lin Gao. Deepface-ideoediting: Sketch-based deep editing of face videos. *ACM Transactions on Graphics (TOG)*, 41(4):1–16, 2022. 2
- [28] Shilong Liu, Zhaoyang Zeng, Tianhe Ren, Feng Li, Hao Zhang, Jie Yang, Chunyuan Li, Jianwei Yang, Hang Su, Jun Zhu, et al. Grounding dino: Marrying dino with grounded pre-training for open-set object detection. *arXiv preprint arXiv:2303.05499*, 2023. 5
- [29] Elizaveta Logacheva, Roman Suvorov, Oleg Khomenko, Anton Mashikhin, and Victor Lempitsky. Deeplandscape: Adversarial modeling of landscape videos. In *Computer Vision—ECCV 2020: 16th European Conference, Glasgow, UK, August 23–28, 2020, Proceedings, Part XXIII 16*, pages 256–272. Springer, 2020. 2
- [30] Chongyang Ma, Li-Yi Wei, Baining Guo, and Kun Zhou. Motion field texture synthesis. In *ACM SIGGRAPH Asia 2009 papers*, pages 1–8. 2009. 2
- [31] Aniruddha Mahapatra and Kuldeep Kulkarni. Controllable animation of fluid elements in still images. In *Proceedings of the IEEE/CVF Conference on Computer Vision and Pattern Recognition*, pages 3667–3676, 2022. 2, 3, 7
- [32] Aniruddha Mahapatra, Aliaksandr Siarohin, Hsin-Ying Lee, Sergey Tulyakov, and Jun-Yan Zhu. Text-guided synthesis of eulerian cinemagraphs. *ACM Transactions on Graphics (TOG)*, 42(6):1–13, 2023. 2, 3, 6, 9
- [33] Tae-Hyun Oh, Kyungdon Joo, Neel Joshi, Baoyuan Wang, In So Kweon, and Sing Bing Kang. Personalized cinemagraphs using semantic understanding and collaborative learning. In *Proceedings of the IEEE International Conference on Computer Vision*, pages 5160–5169, 2017. 3
- [34] Makoto Okabe, Ken Anjyor, and Rikio Onai. Creating fluid animation from a single image using video database. In *Computer Graphics Forum*, pages 1973–1982. Wiley Online Library, 2011. 2
- [35] Yichen Peng, Chunqi Zhao, Haoran Xie, Tsukasa Fukusato, and Kazunori Miyata. Difffacesketch: high-fidelity face image synthesis with sketch-guided latent diffusion model. *arXiv preprint arXiv:2302.06908*, 2023. 2
- [36] William H Press. *Numerical recipes 3rd edition: The art of scientific computing*. Cambridge university press, 2007. 2
- [37] Alec Radford, Jong Wook Kim, Chris Hallacy, Aditya Ramesh, Gabriel Goh, Sandhini Agarwal, Girish Sastry, Amanda Askell, Pamela Mishkin, Jack Clark, et al. Learning transferable visual models from natural language supervision. In *International conference on machine learning*, pages 8748–8763. PMLR, 2021. 7
- [38] Tianhe Ren, Shilong Liu, Ailing Zeng, Jing Lin, Kunchang Li, He Cao, Jiayu Chen, Xinyu Huang, Yukang Chen, Feng Yan, Zhaoyang Zeng, Hao Zhang, Feng Li, Jie Yang, Hongyang Li, Qing Jiang, and Lei Zhang. Grounded sam: Assembling open-world models for diverse visual tasks, 2024. 4
- [39] Robin Rombach, Andreas Blattmann, Dominik Lorenz, Patrick Esser, and Björn Ommer. High-resolution image synthesis with latent diffusion models. In *Proceedings of the IEEE/CVF conference on computer vision and pattern recognition*, pages 10684–10695, 2022. 2, 4, 6
- [40] Nataniel Ruiz, Yuanzhen Li, Varun Jampani, Yael Pritch, Michael Rubinstein, and Kfir Aberman. Dreambooth: Fine tuning text-to-image diffusion models for subject-driven generation. In *Proceedings of the IEEE/CVF Conference on Computer Vision and Pattern Recognition*, pages 22500–22510, 2023. 4
- [41] Xiaoyu Shi, Zhaoyang Huang, Weikang Bian, Dasong Li, Manyuan Zhang, Ka Chun Cheung, Simon See, Hongwei Qin, Jifeng Dai, and Hongsheng Li. Videoflow: Exploiting temporal cues for multi-frame optical flow estimation. In *Proceedings of the IEEE/CVF International Conference on Computer Vision*, pages 12469–12480, 2023. 6
- [42] Ryusuke Sugimoto, Mingming He, Jing Liao, and Pedro V Sander. Water simulation and rendering from a still photograph. In *SIGGRAPH Asia 2022 Conference Papers*, pages 1–9, 2022. 2
- [43] Deqing Sun, Xiaodong Yang, Ming-Yu Liu, and Jan Kautz. Pwc-net: Cnns for optical flow using pyramid, warping, and cost volume. In *Proceedings of the IEEE conference on computer vision and pattern recognition*, pages 8934–8943, 2018. 6
- [44] Christian Szegedy, Vincent Vanhoucke, Sergey Ioffe, Jon Shlens, and Zbigniew Wojna. Rethinking the inception architecture for computer vision. In *Proceedings of the IEEE conference on computer vision and pattern recognition*, pages 2818–2826, 2016. 8
- [45] James Tompkin, Fabrizio Pece, Kartic Subr, and Jan Kautz. Towards moment imagery: Automatic cinemagraphs. In *2011 Conference for Visual Media Production*, pages 87–93. IEEE, 2011. 3
- [46] Patrick von Platen, Suraj Patil, Anton Lozhkov, Pedro Cuenca, Nathan Lambert, Kashif Rasul, Mishig Davaadorj, Dhruv Nair, Sayak Paul, William Berman, Yiyi Xu, Steven Liu, and Thomas Wolf. Diffusers: State-of-the-art diffusion models. <https://github.com/huggingface/diffusers>, 2022. 6
- [47] Andrey Voynov, Kfir Aberman, and Daniel Cohen-Or. Sketch-guided text-to-image diffusion models. In *ACM SIGGRAPH 2023 Conference Proceedings*, pages 1–11, 2023. 2
- [48] Jacob Walker, Carl Doersch, Abhinav Gupta, and Martial Hebert. An uncertain future: Forecasting from static images using variational autoencoders. In *Computer Vision—ECCV 2016: 14th European Conference, Amsterdam, The Netherlands, October 11–14, 2016, Proceedings, Part VII 14*, pages 835–851. Springer, 2016. 2
- [49] Zhou Wang, Eero P Simoncelli, and Alan C Bovik. Multiscale structural similarity for image quality assessment. In *The Thirty-Seventh Asilomar Conference on Signals, Systems & Computers*, 2003, pages 1398–1402. Ieee, 2003. 8

- [50] Jiarui Xu, Sifei Liu, Arash Vahdat, Wonmin Byeon, Xiaolong Wang, and Shalini De Mello. Open-vocabulary panoptic segmentation with text-to-image diffusion models. In *Proceedings of the IEEE/CVF Conference on Computer Vision and Pattern Recognition*, pages 2955–2966, 2023. [2](#)
- [51] Peng Xu, Timothy M Hospedales, Qiyue Yin, Yi-Zhe Song, Tao Xiang, and Liang Wang. Deep learning for free-hand sketch: A survey. *IEEE transactions on pattern analysis and machine intelligence*, 45(1):285–312, 2022. [2](#)
- [52] Xuemiao Xu, Liang Wan, Xiaopei Liu, Tien-Tsin Wong, Liansheng Wang, and Chi-Sing Leung. Animating animal motion from still. In *ACM SIGGRAPH Asia 2008 papers*, pages 1–8. 2008. [2](#)
- [53] Hang Yan, Yebin Liu, and Yasutaka Furukawa. Turning an urban scene video into a cinemagraph. In *Proceedings of the IEEE Conference on Computer Vision and Pattern Recognition*, pages 394–402, 2017. [2](#), [3](#)
- [54] Hu Ye, Jun Zhang, Sibio Liu, Xiao Han, and Wei Yang. Ip-adapter: Text compatible image prompt adapter for text-to-image diffusion models. 2023. [5](#)
- [55] Mei-Chen Yeh. Selecting interesting image regions to automatically create cinemagraphs. *IEEE MultiMedia*, 23(1): 72–81, 2015. [2](#)
- [56] Mei-Chen Yeh and Po-Yi Li. A tool for automatic cinemagraphs. In *Proceedings of the 20th ACM international conference on Multimedia*, pages 1259–1260, 2012. [2](#), [3](#)
- [57] Xiangcheng Zhai, Yingqi Jie, Xueguang Xie, Aimin Hao, Na Jiang, and Yang Gao. Anfluid: Animate natural fluid photos base on physics-aware simulation and dual-flow texture learning. In *Proceedings of the 32nd ACM International Conference on Multimedia*, pages 3323–3331, 2024. [2](#)
- [58] Haichao Zhang, Gang Yu, Tao Chen, and Guozhong Luo. Sketch me a video. *arXiv preprint arXiv:2110.04710*, 2021. [2](#)
- [59] Lvmin Zhang, Anyi Rao, and Maneesh Agrawala. Adding conditional control to text-to-image diffusion models, 2023. [4](#), [7](#)
- [60] Richard Zhang, Phillip Isola, Alexei A Efros, Eli Shechtman, and Oliver Wang. The unreasonable effectiveness of deep features as a perceptual metric. In *Proceedings of the IEEE conference on computer vision and pattern recognition*, pages 586–595, 2018. [8](#)
- [61] Yudian Zheng, Xiaodong Cun, Menghan Xia, and Chi-Man Pun. Sketch video synthesis. 2023. [2](#), [3](#)

Sketch-Guided Motion Diffusion for Stylized Cinemagraph Synthesis

Supplementary Material

7. Motion Field Visualization

The motion field visualization method used in this paper follows the approach presented by Baker et al. [2]. Figure 14 illustrates the color-coding of different motion directions for each pixel in the motion fields, providing an intuitive visualization of flow patterns. Each color corresponds to a specific direction, clearly showcasing pixel-level dynamics and making the generated motion fields more intuitive and easier to understand. The arrows in the color wheel represent the directions in the 2D plane. The intensity of the color represents the speed in that direction.

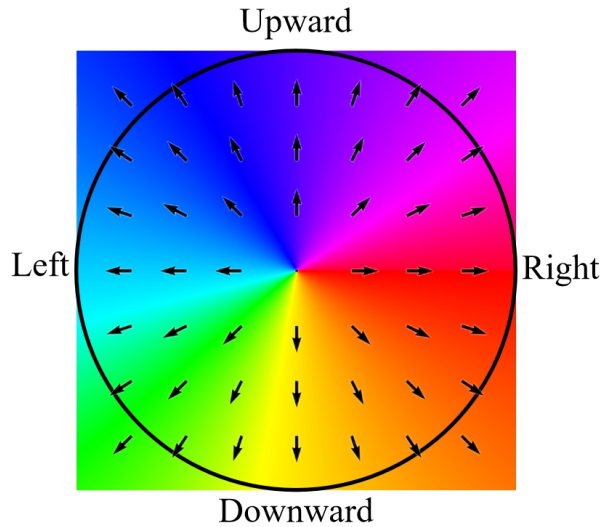


Figure 14. The color wheel of motion field visualization.

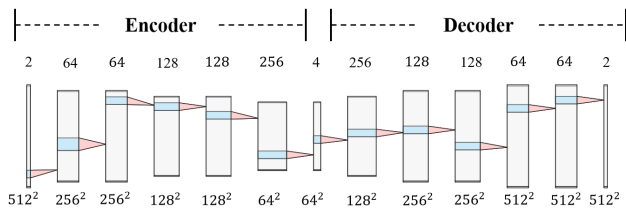


Figure 15. The structure of motion Autoencoder.

8. Motion Autoencoder

Figure 15 illustrates the structure of the motion autoencoder in our Latent Motion Diffusion Model (LMDM). Each module of the autoencoder integrates convolutional layers and ReLU activation functions to effectively capture both spatial and temporal motion features. The motion autoencoder

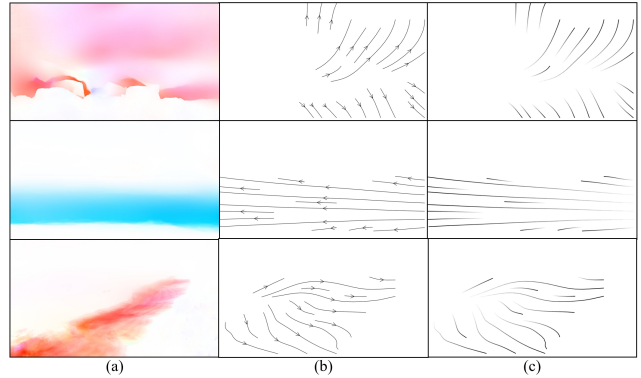


Figure 16. The streamlines (a) are extracted from the motion fields and then converted into gradient gray lines to serve as ground truth motion sketches during LMDM’s training (b).

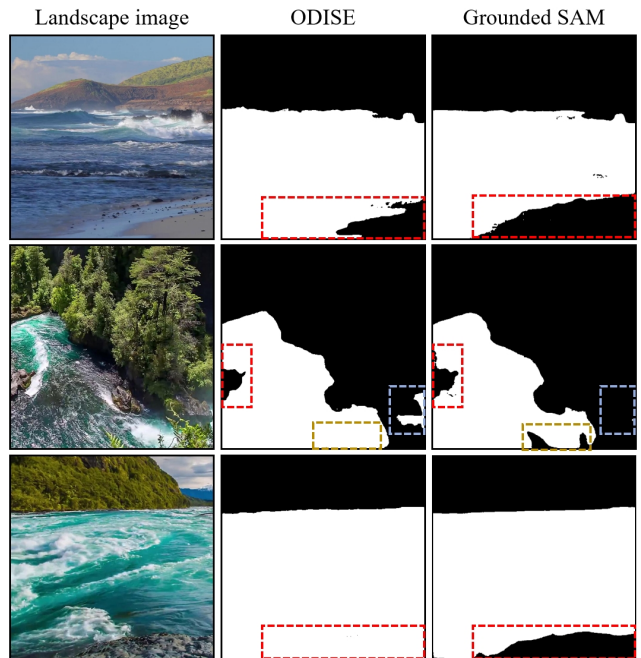


Figure 17. Ablation Study (fluid mask extraction). Guided by text prompt, Ground SAM can extract fluid masks with clearer and more precise edges compared to ODISE, which highlighted in the colored boxes.

was trained independently, with hyperparameters including a learning rate of $lr = 1 \times 10^{-4}$ and a batch size of 16, balancing training stability and efficiency. This design and training process enables the autoencoder to generate compact and expressive latent motion representations, suitable for downstream diffusion-based synthesis tasks.

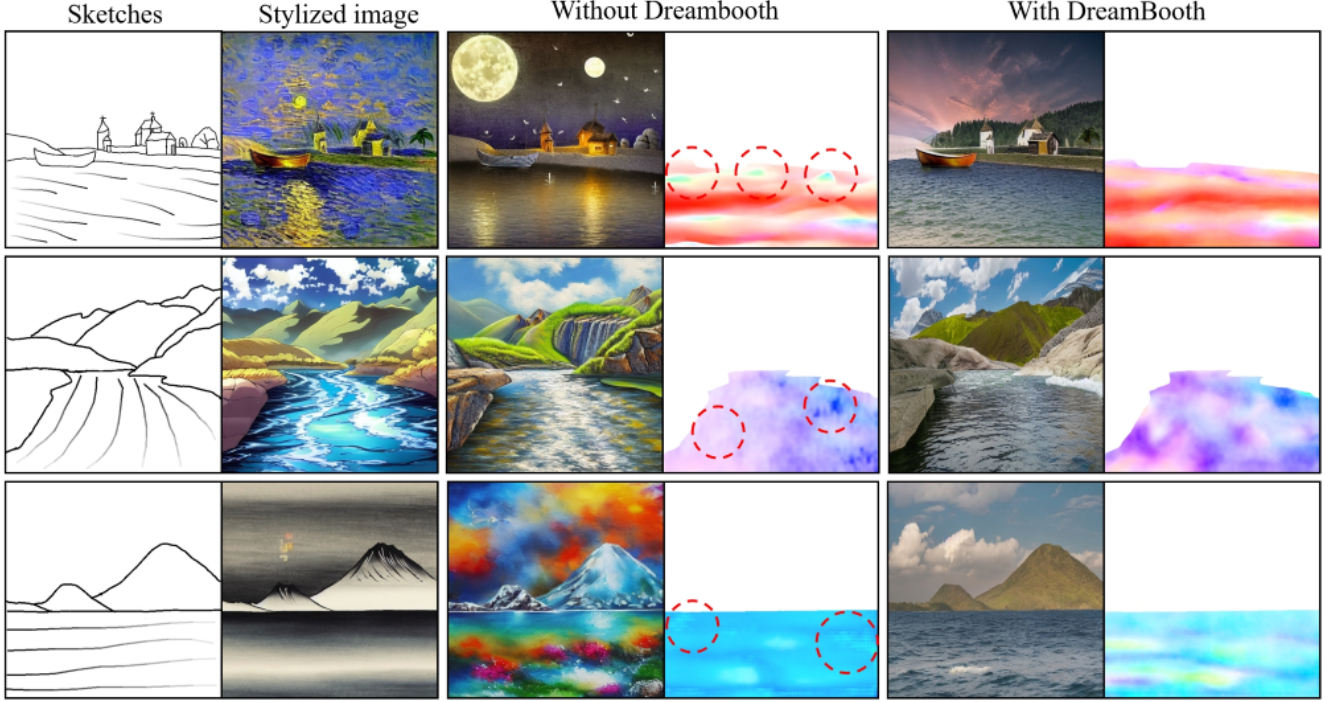


Figure 18. Ablation study on realistic landscape image for motion field prediction.

9. Streamlines Extraction

The motion sketch used herein consists of streamlines extracted from given 2D motion field data. Streamlines represent the trajectory of fluid particles at a given instant in time. This offers an effective approach for characterizing a complex motion field. The Runge-Kutta method[36] is a common method to calculate the streamlines. In our study, we focus on extracting streamlines from a single velocity field, hence the equations are defined as follows:

$$\begin{aligned} x_{n+1} &= x_n + \frac{h}{6}(k_{1x} + 2k_{2x} + 2k_{3x} + k_{4x}) \\ y_{n+1} &= y_n + \frac{h}{6}(k_{1y} + 2k_{2y} + 2k_{3y} + k_{4y}) \end{aligned} \quad (7)$$

$$\begin{cases} k_{1x} = f_x(x_n, y_n) \\ k_{1y} = f_y(x_n, y_n) \\ k_{2x} = f_x(x_n + \frac{h}{2}k_{1x}, y_n + \frac{h}{2}k_{1y}) \\ k_{2y} = f_y(x_n + \frac{h}{2}k_{1x}, y_n + \frac{h}{2}k_{1y}) \\ k_{3x} = f_x(x_n + \frac{h}{2}k_{2x}, y_n + \frac{h}{2}k_{2y}) \\ k_{3y} = f_y(x_n + \frac{h}{2}k_{2x}, y_n + \frac{h}{2}k_{2y}) \\ k_{4x} = f_x(x_n + hk_{3x}, y_n + hk_{3y}) \\ k_{4y} = f_y(x_n + hk_{3x}, y_n + hk_{3y}) \end{cases} \quad (8)$$

where x_n, y_n are given as the particle position at status n , x_{n+1}, y_{n+1} are the particle position at status $n + 1$. h is given the time step, k_{1x}, k_{1y} are the slopes in x and y

direction at start point, $k_{2x}, k_{2y}, k_{3x}, k_{3y}$ are the slopes at the middle points, k_{4x}, k_{4y} are the slopes at the end point. f_x and f_y represent the x and y components of the velocity field. The original streamlines are visually represented using arrows, which lack prominent directional features. Therefore, this paper converts them into gradient gray lines to enhance their vector information, as shown in Figure 16.

10. Ablation Study

To assess the impact of our design choices in the proposed method, we conducted a series of ablation studies, specifically focusing on the effectiveness of fluid mask generation and the generated realistic landscape images in sketch-guided motion field prediction stage.

10.1. Fluid Mask Extraction

This paper adopts a state-of-the-art text-guided extraction method, Grounded SAM. Compared to ODISE [50], Grounded Segment Anything Model (SAM) demonstrates superior performance in accurately identifying fluid regions within realistic landscape images. It excels in generating fluid masks with precise edges, particularly at the boundaries between oceans, rivers, and embankments, as shown in Figure 17. In contrast, T2C’s mask generation method utilizes ODISE masks to extract regions from the self-attention maps obtained during the image generation process of the text-to-image diffusion model, primarily for cutting error

Figure 20. Stylized cinemagraphs generated by our framework. (The generated stylized cinemagraphs are embedded and better viewed using Adobe Reader.)

parts. However, this approach cannot be applied to existing images, whereas the Grounded SAM method is compatible with both existing and generated landscape images. In addition, Grounded SAM demonstrates better time efficiency, with average processing times of 374.090 seconds for ODISE and 16.301 seconds for Grounded SAM.

10.2. Realistic Landscape Image Conditioning

The realistic images are generated using an LDM fine-tuned with DreamBooth for motion fields prediction. We conduct an ablation study on motion field generation, comparing results using realistic images generated by the fine-tuned LDM and the original LDM as shown in Figure 18. When using images generated by the original LDM without DreamBooth fine-tuning as input, the resulting motion fields maintain the overall direction but lack detailed flow variations, exhibiting discontinuities and erroneous regions, highlighted by red circles. This highlights the effectiveness

of DreamBooth in producing realistic landscape images for motion field prediction.

11. Examples of Stylized Cinemagraphs

Figure 20 showcases a variety of stylized cinemagraphs generated by our framework, demonstrating its ability to generate the dynamic motion of flowing skies and clouds under the provided motion sketches. These results emphasize the adaptability of our approach in handling various styles and motion scenarios, making it suitable for both artistic and realistic applications.